REVIEW

Dynamics of Recent Climate Change in the Arctic

Richard E. Moritz,[1]* Cecilia M. Bitz,[1] Eric J. Steig[2]

The pattern of recent surface warming observed in the Arctic exhibits both polar amplification and a strong relation with trends in the Arctic Oscillation mode of atmospheric circulation. Paleoclimate analyses indicate that Arctic surface temperatures were higher during the 20th century than during the preceding few centuries and that polar amplification is a common feature of the past. Paleoclimate evidence for Holocene variations in the Arctic Oscillation is mixed. Current understanding of physical mechanisms controlling atmospheric dynamics suggests that anthropogenic influences could have forced the recent trend in the Arctic Oscillation, but simulations with global climate models do not agree. In most simulations, the trend in the Arctic Oscillation is much weaker than observed. In addition, the simulated warming tends to be largest in autumn over the Arctic Ocean, whereas observed warming appears to be largest in winter and spring over the continents.

It is now well established that important changes occurred in Arctic climate during the 20th century, including a marked increase of surface air temperature (SAT) during 1970–2000 (Fig. 1A) (*1*–*3*). The warming was correlated with important but less well-documented changes in many other Arctic climate and environmental variables, such as precipitation, sea-ice extent, snow cover, permafrost temperature, and vegetation distribution (*2*, *4*, *5*). Because these changes had considerable impacts on people and ecosystems in the Arctic and may also have global impacts through a variety of climate feedback mechanisms, it is important to know whether they will continue in the future. To project future Arctic climate change with confidence requires an understanding of how radiative forcing [e.g., from anthropogenic greenhouse gas (GHG) concentrations] and internal variability (from the internal dynamics of the climate system) contributed to the recent trends.

As is increasingly recognized, the response of the climate system to radiative forcing may be closely linked to free modes of internal variability, both in an observational and a dynamical sense. For example, the Arctic Oscillation (AO) (*6*) has been simulated successfully as a purely free internal mode in atmospheric general circulation models (GCMs) (*7*, *8*). Also, the spatial pattern of the recent trend in Arctic SAT (Fig. 2A) strongly resembles the SAT signature of the AO (Fig. 2B), whereas the AO index exhibited a substantial positive trend (Fig. 1B). These correspondences, along with physical reasoning supported by some GCM experiments, support the hypothesis that the recent trend in the AO is a consequence of anthropogenic radiative forcing that somehow excites this free mode of variability (*9*–*12*). Though satisfactory understanding of forced and free variability of Arctic climate remains elusive, substantial progress has been made in the past 5 years or so on the basis of statistical and dynamical analysis of historical observations, paleoclimate reconstructions, physical theories, and numerical climate modeling. Here, we summarize recent progress in each of these areas, discuss outstanding questions, and explore the potential for predicting future changes.

Evidence from Historical Observations

A sizable fraction of Arctic climate variations can be described in terms of one or more characteristic spatial patterns or "patterns of variability." In this section, we describe the important patterns exhibited by historical observations of Arctic surface temperature over the 20th century and by simulations of climate model responses to prescribed forcing. We include patterns resulting from natural modes of variability as well as those that reflect spatially dependent physical properties and mechanisms.

In recent decades, sea-level pressure (SLP) in the Arctic decreased more than anywhere else in the Northern Hemisphere (NH) (*13*). Much of this decrease can be linked to the AO. The AO is defined as the leading empirical orthogonal function (EOF) of wintertime monthly mean SLP poleward of 20°N (*6*); its state is described by an index that measures the projection of SLP onto the EOF. The AO pattern has SLP anomalies of one sign over most of the Arctic and of the opposite sign over the mid-latitude Atlantic and Pacific Oceans. In the high–AO index state, surface westerly winds are enhanced in a belt circling the Arctic from about 50° to 70°N. In the late 20th century, the AO index exhibited an upward trend (*14*) and the amplitude of interdecadal oscillations increased in comparison to the record from about 1900–70 (Fig. 1B) (*15*).

The pattern of SAT that is associated with the AO has anomalies of the same sign as the AO index in Siberia and anomalies of the opposite sign in Alaska and in the Labrador region (*6*). The upward trend in the AO from 1968–97 accounts for half of the observed wintertime warming over Eurasia (*14*). Temperature measurements over the Arctic Ocean are sparse and prone to high uncertainty. During the limited record of the past 20 years, the AO accounted for more than half of both the warming over the eastern Arctic Ocean and the cooling over the Labrador Sea (*16*).

The circulation of Arctic sea ice is correlated with the AO such that during periods of high AO, there is reduced convergence of ice area in the eastern Arctic Ocean, a retreat of ice in the Greenland and Barents Seas, and an increased export of ice area through Fram Strait (*17*–*19*). Modeling studies show similar relations between atmospheric circulation and ice volume as well (*20*). The estimated correlation between annual ice export and the AO-related North Atlantic Oscillation (NAO) index is significantly larger over the post-1977 period than for the preceding two decades (*21*). Over the past few decades, summer ice concentration in the eastern Arctic Ocean and the Barents and Nordic Seas has declined sharply (*22*), a trend that has been associated with the trend in the AO (*18*, *19*). In addition, a host of other climate variables has been related to the AO [see reviews in (*2*, *4*, *23*)].

The NAO is a pattern with considerable explanatory power in the Arctic. The NAO pattern overlaps with the AO pattern and, consequently, they are highly correlated over time. It remains to be seen whether the AO and the NAO are distinct phenomena (*24*–*27*). The AO is also known as the NH annular mode (NAM), to distinguish it from its counterpart in the Southern Hemisphere (*28*). For this review, we treat the AO, NAM, and NAO as one phenomenon, and we use the AO designation, except where explicit distinctions are essential.

Another important pattern in the Arctic is the poleward increase of the response of SAT

[1]Polar Science Center, [2]Quaternary Research Center, University of Washington, Seattle, WA 98105–6698, USA.

*To whom correspondence should be addressed. E-mail: dickm@apl.washington.edu

to climate forcing. This so-called polar amplification is usually associated with the response of SAT to an increase in radiative forcing as simulated by GCMs (Fig. 2C) (*29*, *30*), though polar amplification is also seen in the variance of SAT in both observations and models (*31*). Using newly available Siberian station data, Polyakov *et al.* (*32*) estimated that the recent surface warming trend was larger poleward of 62°N than over the rest of the hemisphere, although not at the 95% confidence level (i.e., not significantly). This relation also appears to hold for the three major multidecadal trends shown in Fig. 1A: 1920–40, 1940–70, and 1970–2000.

The Arctic actually cooled substantially for about two decades between 1940–60, when trends were small elsewhere (Fig. 1A). It is not yet known why Arctic temperatures departed from the NH mean during this time, although a similar fluctuation occurred in a climate simulation using a coupled model forced by GHG and sulfate aerosol levels of the 20th century (*33*). The modeled cooling resulted from internal variability. Others have speculated that Arctic tropospheric aerosols and changes in total solar irradiance played a strong role (*34*, *35*). The AO index (Fig. 1B) also was below average from 1940–60. The AO and polar amplification patterns share some overlap as the temperature pattern associated with the AO exhibits polar amplification (Fig. 3). On the basis of this association between SAT and AO, it is possible that the AO played a role in the mid-century cooling of the Arctic.

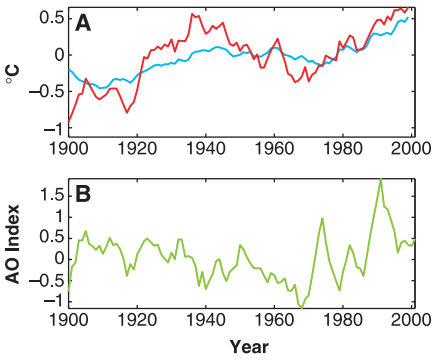

Fig. 1. (**A**) Annual mean SAT for the Northern Hemisphere (blue) and for the Arctic (60° to 90°N, red) from gridded land-station data (*86*). Ocean stations are excluded because few exist in the Arctic. (**B**) Annual mean values of the AO index (*28*). Data are smoothed with a 5-year running mean filter.

Next we consider a pattern that reflects the different physical properties and mechanisms of ocean and land surfaces. For example, observed low frequency variance and trends in SAT are larger over the continents than over the oceans annually (Fig. 2A) and in winter and spring (*13*, *36*), mainly due to the greater effective heat capacity of the upper ocean (*31*). The observed cold ocean–warm land (COWL) pattern has been cited as an indication that the SAT trends are related to the changes in atmospheric circulation (*37*). Currently the focus of research has shifted to the AO, the SAT pattern of which resembles the COWL pattern, as the link between SAT trends and circulation changes.

Fluctuations in the North Atlantic thermohaline circulation (THC) are a likely source of low-frequency temperature changes in the northern North Atlantic. The THC and the Gulf Stream transport heat from the south into the northern North Atlantic. Although direct evidence linking the observed surface temperature to the THC changes is lacking, one modeling study estimates that SAT over the northern North Atlantic, Greenland, and Scandinavia (*38*) can be altered by about 1°C on decadal time scales due to fluctuations in the intensity of the THC in its present-day regime. Modeling studies also reveal a potentially strong connection between the THC and sea-ice export (*39*, *40*), with an associated response in sea-ice extent and surface temperature (*40*).

When forced with increasing GHG, global climate models typically warm less in the northern North Atlantic than in other locations at the same latitude on ocean or land (Fig. 2C). Vertical mixing reaches a local maximum there due to relatively weak stratification, giving rise to high thermal inertia (*30*). Many of the climate models simulate a weakened THC in response to GHG increase, and this may also contribute to the relatively weak warming in the northern North Atlantic (*41*).

Essentially, three spatial patterns emerge from the discussion. One is the observed pattern (Fig. 2A); another is the temperature pattern associated with the AO (Fig. 2B); and a third is the pattern associated with enhanced GHG simulations (Fig. 2C). All three patterns exhibit some polar amplification and COWL, so there is quite a bit of overlap among them. However, there is a notable exception over the western Arctic Ocean (not shown due to a data void in our Fig. 2A), where there is documented cooling (*16*, *42*) that appears only in the observed pattern. There are also three key features that stand out in the time series of 20th century Arctic average SAT: warming from 1920–40, cooling from 1940–70, and the recent warming from 1970–2000. The amplitude of each swing is larger in the Arctic than over the NH as a whole.

Physical Processes and Forcing Functions

External forcing and internal dynamics contribute to the observed temporal and spatial variations of Arctic climate. The forcing factors relevant to 20th-century climate may be divided into anthropogenic, chiefly increased GHG, increased sulfate aerosols, and decreased stratospheric ozone, and natural factors, such as vari-

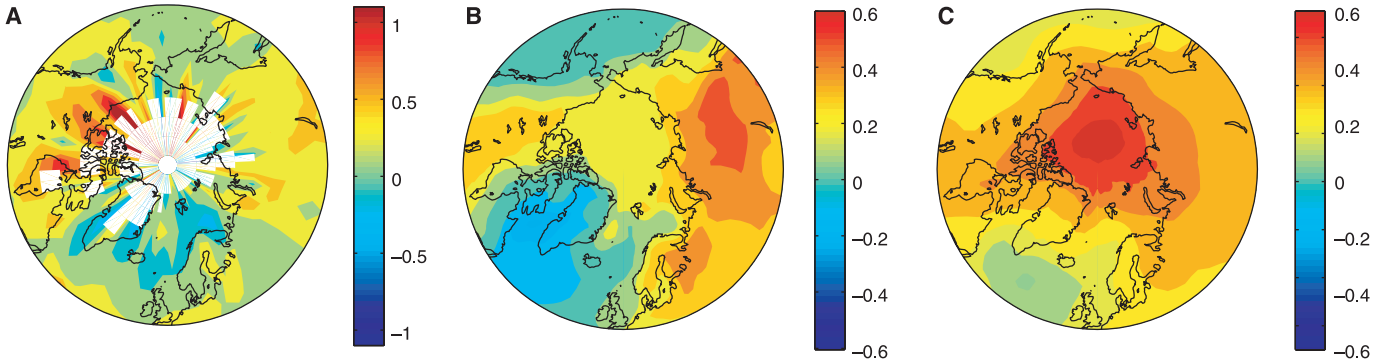

Fig. 2. Trends in SAT (**A**) estimated from observations, for all months from 1971–2000. [Estimates were provided by W. Chapman (*36*).] (**B**) SAT trends estimated from the National Centers for Environmental Prediction/National Center for Atmospheric Research (NCEP/NCAR) reanalysis (*87*), regressed on the AO index for all months from 1948–2002 and multiplied by the trend in the winter AO index. (**C**) SAT trends simulated as a response to doubling carbon dioxide levels, averaged over 19 models participating in the Coupled Model Intercomparison Project (*88*). The trend was calculated from the temperature difference averaged for all months in years 60 to 80 from simulations with a transient 1% increase per year in carbon dioxide minus the 80-year average from a control run with preindustrial carbon dioxide levels divided by 7 decades. [The values were provided by J. Räisänen.] Units in (A), (B), and (C) are °C per decade.

ations in total solar irradiance and volcanic aerosols [chap. 6 of (*41*)]. In general, the forced response and the internal variability of climate are affected by feedback mechanisms [chap. 7 of (*41*)] and by geographical variations of surface type. Insight may be gained by considering how physical processes affect the relations between these climate-forming factors and the spatial and temporal patterns of Arctic climate change.

In the real climate system, many factors vary simultaneously and controlled experiments are impossible. Thus, much of our knowledge of mechanisms derives from theory and simulations performed with global models. Simulations of 20th-century climate produce reasonable facsimiles of the multidecadal trends in zonal mean surface temperature over the NH (*9*, *33*, *41*, *43*, *44*) and the Arctic (*45*). The agreement between simulated and observed 20th-century trends is somewhat better when forcing includes total solar irradiance and volcanic aerosols, in addition to the more commonly prescribed GHG and sulfate aerosol forcing. Still, questions remain because some simulations have produced a good match to observations using only two of the five forcings, with a fortuitous realization of natural variability (*33*, *43*, *44*).

The full spatial pattern of GCM response to 20th-century forcing is less well-documented in the literature than the zonal average trends, especially in the Arctic; here, we rely mainly on inference by scaling back the results of CO_2 doubling experiments (Fig. 2C) for comparison with 20th-century Arctic observations. The most obvious simulated feature is the polar amplification of SAT change, with a maximum centered squarely on the Arctic Ocean. Also evident are the equatorward extensions of high-latitude surface warming over the continents, with relatively smaller changes over the oceanic sectors, especially the North Atlantic.

Global spatial patterns of estimated direct radiative forcings during 1750–2000 [p. 389 of (*41*)] do not resemble the patterns of observed and simulated warming shown in Fig. 2. In particular, none of the radiative forcings indicate polar amplification of warming

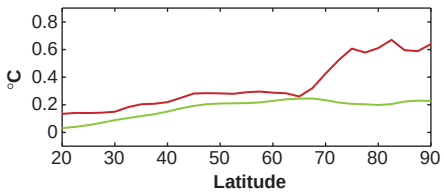

Fig. 3. Green curve, zonal mean of SAT regressed on the AO index and multiplied by the trend in the AO index. Red curve, trend of zonal mean of SAT. Both curves computed from monthly NCEP/NCAR reanalysis, 1948–2002, with trends expressed as °C per 30 years (*87*).

through direct effects of local radiation. This suggests that feedback mechanisms together with changes in heat transported by the atmosphere and ocean are important contributors to the simulated pattern.

Positive feedback mechanisms, associated with the surface heat budget and changing albedo of snow cover and sea ice, account for much of the simulated polar amplification pattern. The basic mechanism as represented in a GCM has been understood for some time (*29*). Over sea ice positive perturbations in the surface heat budget may be forced directly by enhanced GHG and indirectly by warmer, moister air transported into high latitudes in response to GHG-induced anomalies of heating and convection in lower latitudes. These perturbations drive warming, enhance summer melting, and diminish winter freezing of the sea ice, so that surface albedo, which is modeled as a function of temperature and ice thickness, decreases. The additional absorbed insolation produces further warming and melting, so that the equilibrium thickness of the ice is much smaller than it would have been without the albedo feedback. In autumn and early winter, the thin ice has lost much of its ability to thermally insulate the ocean, so there is a substantial increase in upward heat conduction that heats the air, producing the geographical and seasonal maximum SAT response to GHG. This enhanced conduction in autumn drives rapid freezing at the bottom of the sea ice. Because thinner ice grows faster, anomalies of ice thickness tend to be damped out as winter progresses (*46*). A positive albedo feedback also operates in the model snow cover on land (*29*). But without the winter heat source represented by seawater at the freezing point, the maximum SAT response over the snow is smaller and occurs in the spring with early melt of the snowpack.

The extent to which SAT response resembles polar amplification and COWL depends on the time scale of the forcing, as seen in differences between the transient and equilibrium response of climate models to CO_2 doubling (*30*). COWL is more pronounced in the transient experiment as ocean heat uptake buffers the change of surface temperature.

In its high index state, the AO is characterized by anomalously strong westerlies around the perimeter of the Arctic (*28*). These anomalous wind velocities have a large component perpendicular to the climatological isotherms. This implies anomalous horizontal temperature advection. In winter, this advection tends to warm the continents more than it tends to cool the oceans, because of the larger thermal inertia of the oceans. Thus, a COWL-like temperature signature is associated with the AO, but it is modified by undulations in the patterns of AO winds and climatological air temperatures. The AO contribution to advection of mean temperature, integrated through the troposphere, exhibits a spatial pattern (not shown) of anomalous heating remarkably similar to the AO SAT pattern (Fig. 2B), in support of this interpretation (*28*). The reduction in wintertime continent-ocean temperature contrast associated with high AO index results in an overall increase in zonal mean temperature. Because both the anomalous AO surface winds and the climatological continent-ocean temperature difference increase with latitude, it is perhaps not surprising that the AO pattern exhibits polar amplification (Fig. 3).

Although the AO is defined as the first EOF of sea level pressure, it may be characterized equally well in terms of the latitude-height cross section of the zonal mean zonal wind in the NH (*14*, *47*). This characterization is useful in theories of AO dynamics, which treat the climatological zonal mean zonal wind as a basic state. Perturbations superimposed on this zonally symmetric state are called "eddies," and they may be analyzed using linear wave theory (*48*). The high-minus-low composite AO anomaly cross section exhibits an enhancement of the westerly polar night jet stream in the lower stratosphere, centered around about 70°N latitude, with a smaller, negative anomaly near the 150-hPa pressure level in the subtropics. Lobes from both these anomaly extrema extend to the surface. In individual large-amplitude, high- and low-index events, stratospheric wind anomalies are observed to propagate downward, and they are correlated on time scales of weeks with zonal wind anomalies at the surface (*47*, *49*).

Currently, there is no generally accepted theory for the existence of the AO (*27*). But diagnostic analyses and partial theories indicate that the following features of the atmospheric circulation are important: the polar night jet stream in the Arctic stratosphere, the eddy transport of zonal momentum by cyclone-scale waves and planetary waves, and the mean meridional circulation driven by this eddy transport (*7*, *11*, *50*–*52*).

Planetary waves are characterized by horizontal length scales comparable to the radius of Earth, and they propagate both horizontally and vertically from their source regions. They may be forced thermally by variations in surface heating and mechanically by flow over mountains (*48*). According to theory and observations, the propagation paths of these waves depend on the basic state pattern of zonal mean zonal winds (*7*, *53*). When the AO index varies, so does the basic state, which then influences propagation. Diagnostic and theoretical results indicate that planetary waves exhibit anomalous equatorward propagation during high-AO events (*7*). Analysis of the wave properties shows that equatorward propagation is accompanied by an anomalous poleward flux of eddy

zonal momentum (*50*). This flux tends to accelerate the already anomalously strong westerlies in the high latitudes, providing a self-reinforcing mechanism for the AO. It has been suggested that this mechanism, and an analogous one that affects vertical propagation, may be crucial in explaining the large amplitude and long duration of AO anomalies (*7*, *11*). Vertically propagating planetary waves tend to transport heat and negative zonal momentum anomalies into the stratosphere, but strong westerlies (high AO) inhibit this transfer (*53*, *54*). Therefore, a high-AO index allows the stratospheric vortex to strengthen as it cools toward radiative equilibrium. Enhanced upper westerlies in the high AO state drive a thermally indirect mean meridional circulation with rising motions and enhanced surface westerlies around the Arctic (*7*), consistent with diagnostic analysis of the potential vorticity equation in each atmospheric layer (*55*).

Advances in dynamical understanding of intraseasonal AO variability have not revealed the causes of the recent trend in the AO, which continues to be debated. Increased anthropogenic GHG and decreased stratospheric ozone are thought to cool the lower stratosphere in high latitudes [chap. 9 of (*41*)], and therefore have the potential to increase the AO index. The control simulations of most climate models exhibit robust AO-like variability on intraseasonal to interannual time scales, and several enhanced GHG experiments result in trends of the simulated AO (*9*, *10*, *56*, *57*). But only one model (*9*) that has enhanced vertical resolution in the stratosphere produced AO trends of realistic magnitude. And even this model does not reproduce the observed cooling trend in the stratosphere (*57*). In another model, the AO is insensitive to changes in vertical resolution of the stratosphere (*58*). In most of the simulations of AO response to GHG, stratospheric ozone amount is fixed. Additional research is needed to determine whether current GCMs lack the physics essential to the low-frequency response of the AO to GHG forcing or whether only a small portion of the observed trend is in fact a forced response to GHG increase. In any case, it is also important to determine how much of the non-GHG trend was driven by other radiative forcing, such as total solar irradiance, ozone amount, sulfate aerosols, and volcanic aerosols, and how much is free variability.

A variation on this theme is that the upward trend of the NAO since 1950 is a remote response to the observed multidecadal upward trend of sea-surface temperature (SST) in the Indian and Pacific Oceans (*12*). The trend in tropical SST could arise in principle from intrinsic ocean-atmosphere variability or could be forced radiatively by enhanced GHG or solar irradiance. Either way, the positive SST anomalies drive anomalies of tropical atmospheric convection, which can affect the generation of planetary waves. Given the high correlation between AO and NAO, it is possible that the trend in both indices could be driven by enhancement of the source function for planetary waves, due to tropical greenhouse warming. Tropical convection is difficult to simulate well in GCMs (*59*).

Evidence from Paleoclimate Reconstructions

Historical observations suggest that a large fraction of recent climate change in the Arctic shares some common features with a few recognized spatial patterns (*14*). However, as summarized above, understanding of the underlying physics that causes these patterns remains insufficient, both for uniquely attributing observed variations to forcing functions and for predictive purposes. In this context, the information available from the paleoclimate record provides useful additional insight. Paleoclimate data provide a longer time frame within which to view natural variability and a means to examine the response of the system to different radiative forcing conditions, including those prior to influence of anthropogenic CO_2 emissions.

It is of particular interest to consider whether paleoclimate data support the concept that the recent Arctic warming is truly exceptional in the context of natural variations. An important milestone in addressing this question is the synthesis paper of Overpeck *et al.* (*34*), which summarizes 29 independent paleo-data sets from the perimeter of the Arctic that can be related empirically to Arctic temperature. Though historical data do not prove that the rate of Arctic warming in the past two decades has been exceptional (*2*), the paleo-data show that, as a whole, the 20th century was exceptionally warm relative to the previous three centuries (at least). This result is echoed by more comprehensive data compilation and climate reconstruction work (*60*, *61*), which provides an estimate of NH average temperature change through the past 1000 years. A more recent reconstruction (*62*), which suggests that the peak warmth of the Medieval Warm Period (approximately 1000 A.D.) may have rivaled that of the 20th century, nevertheless underscores the conclusion that the 20th century is exceptional in at least the past several hundred years. The Esper *et al.* (*62*) results, based primarily on data from high latitudes, also suggest that polar amplification is not only a feature of the most recent warming but also characteristic of low-frequency climate variations in general. Thus, there appears to be little ambiguity to the statement that average Arctic SAT in the past century—and the past few decades in particular—has been exceptionally high and that the Arctic warming has been greater than that at low and middle latitudes of either hemisphere. [The Antarctic, in contrast, has experienced average cooling; see (*63*) and (*64*) for recent analyses.]

The importance of the recent upward trend and increased variability of the AO, relative to the record of preindustrial climate, is more ambiguous. No published paleoclimate work has attempted to reconstruct the AO, but several attempts have been made to reconstruct the NAO index over the past several hundred years with the use of a combination of paleoclimate proxy and historical climate data, where available (*65*–*68*). The various reconstructions are not well correlated with one another on interannual time scales, which may reflect that AO-NAO teleconnection patterns are not stationary (*69*). Virtually all of the records show a strong trend in the past three decades that appears exceptional in the context of the past few hundred years. In contrast, the amplitude of the NAO interdecadal variability in the late 20th century does not appear to be atypical of that during most of the past 400 to 500 years in any of the reconstructions. As with average temperature, it appears that the 20th century was exceptional, but decadal and shorter frequency variations in the AO do not demonstrably fall outside the range of natural variability.

The recent trend in the AO is hypothesized to be a response to radiative forcing (*9*–*12*), rather than a low-frequency mode of internal dynamics. The latter would be unlikely to persist for more than two decades, unless some atmosphere-ocean coupling is at work. There is support for the radiative forcing hypothesis in paleoclimate records, which indicate that century to millennial-scale variations in North Atlantic climate over the past few thousand years correspond in timing with solar irradiance changes (*70*). Records of atmospheric circulation changes from Greenland ice cores indicate reduced zonal flow, consistent with the low phase of the AO when solar irradiance was low and Europe was cold, such as during the Little Ice Age [(LIA) from the years roughly 1400–1900] (*71*). These results are consistent with the much earlier suggestion of an NAO-like pattern in the timing of retreat and advance of alpine glaciers during the LIA (*72*). However, the results do contrast with evidence from marine sediment proxy records of iceberg and sea-ice rafting and SST, which implies a uniform climatic response across the North Atlantic for the LIA, rather than the AO-like pattern implied by other evidence (*73*). This apparent discrepancy has not been resolved.

There are several plausible mechanisms through which radiative forcing would project onto the various patterns, and it remains to be seen which of these are important. The paleoclimate data can be used in support of at least one of the candidate hypotheses: that the most direct impact of radi-

ative forcing changes is on tropical SST, which then influences the AO through planetary wave dynamics. Recent reconstructions of climate variations during the last glacial period show that the millennial-scale fluctuations in temperature that are so prominent in North Atlantic paleoclimate records (*74*, *75*) coincided in timing with low-frequency, El Niño–Southern Oscillation (ENSO)–like variations in the pattern of tropical Pacific SST (*76*, *77*). This interpretation of the paleoclimate data marks a major departure from earlier research, which has strongly supported the notion that changes in the THC are the primary driver of millennial-scale climate variations in the Arctic (and globally) (*78*). Certainly, there is abundant evidence for major THC changes associated with each of the major climate fluctuations of the last glacial period (*79*, *80*). However, there is little evidence that THC changes were associated with the smaller magnitude climate variations of the past thousand years, such as the LIA (*81*). Thus, it seems unlikely (though certainly not disproven) that changes in THC played a large role in the recent Arctic warming.

Patterns of Variability and Future Prediction

Climate change in the Arctic may be described in terms of spatial patterns that are associated with a variety of physical processes. There is much overlap among the patterns that result from variations in the AO, changes in the THC, and differences in the heat capacity of ocean and land. Identification of mechanisms based solely on spatial patterns is, therefore, not easy. However, some patterns, and in particular that of the AO, exhibit temporal behavior resulting plausibly from a combination of free and forced variation and offer potential both for understanding of fundamental dynamics and for developing predictive capability (*26*). GCMs successfully reproduce the AO pattern and variability on daily to interannual time scales (*7*, *9*, *10*). Also, when forced with increasing GHG levels, most models respond with an increase in the AO, but at a rate that is significantly smaller than observed (*57*). For this reason, the warming pattern in models shown in Fig. 2C may not be strongly related to the AO. The models tend to show strong polar amplification from positive feedbacks associated with sea ice and snow.

GCMs that simulate time-dependent sea-ice variables uniformly show polar amplification of GHG warming in the NH. But at high latitudes, differences between the amplitude of warming simulated by different models are maximized (*41*). The wide range of model response is sometimes blamed on the physical formulations of the sea-ice component (*82*). We note that there is only a weak relation between the basic state of sea ice (i.e., ice extent and thickness in the control climate) and the high-latitude climate sensitivity among global models (*83*–*85*). Further explanation of disagreements among climate models remains a problem.

Consistent with sea-ice albedo positive feedbacks, climate models simulate maximum greenhouse warming in autumn over the Arctic Ocean, when thinner and less extensive sea ice has the greatest impact on the atmosphere and before it is partly obscured by snowfall and sea-ice growth. However, the observed maximum warming occurs in winter and spring, when the AO variability is larger and when the polar vortex and/or jet stream are strong enough to provide a conduit for changes in feedbacks involving atmospheric dynamics. The relations between the AO and simulated and observed SAT trends in the Arctic merit further research.

Paleo-data show that Arctic SAT in the 20th century was exceptionally high compared with the previous 300 years and that this was likely caused by GHG forcing, although there is no consensus on the cause of the Arctic cooling during 1940–60. In the past 30 years, the AO has played a key role in Arctic climate change. It is not clear whether the AO has been as important before this period or how it will contribute to the future. Most GCMs underestimate the magnitude of the trend in the AO when forced with 20th-century radiative forcing and continue to simulate weak trends under future forcing scenarios. In addition, these models tend to produce a tremendous spread in their predicted future warming in the Arctic. Clearly, the spread in warming cannot be attributed to their simulation of the AO. It is more likely that the disagreement stems from the parameterizations of surface albedo, cloud processes, and other feedback mechanisms in the high latitudes.

References and Notes

1. P. D. Jones, M. New, D. Parker, S. Martin, I. Rigor, *Rev. Geophys.* **37**, 173 (1999).
2. M. C. Serreze *et al.*, *Clim. Change* **46**, 159 (2000).
3. J. K. Eischeid, C. B. Baker, T. R. Karl, H. F. Diaz, *J. Appl. Meteorol.* **34**, 2787 (1995).
4. J. Morison, K. Aagaard, M. Steele, *Arctic* **53**, 359 (2000).
5. SEARCH SSC, *SEARCH: Study of Environmental Arctic Change, Science Plan*, J. Morison *et al.*, Eds. (Univ. of Washington, Seattle, 2001), pp. 1–89.
6. D. W. J. Thompson, J. M. Wallace, *Geophys. Res. Lett.* **25**, 1297 (1998).
7. V. Limpasuvan, D. L. Hartmann, *J. Clim.* **13**, 4414 (2000).
8. A. W. Robertson, *J. Clim.* **14**, 3240 (2001).
9. D. T. Shindell, R. L. Miller, G. A. Schmidt, L. Pandolfo, *Nature* **399**, 452 (1999).
10. J. Fyfe, G. Boer, G. Flato, *Geophys. Res. Lett.* **26**, 1601 (1999).
11. D. L. Hartmann, J. M. Wallace, V. Limpasuvan, D. W. Thompson, J. R. Holton, *Proc. Natl. Acad. Sci. U.S.A.* **97**, 1412 (2000).
12. M. P. Hoerling, J. W. Hurrell, T. Xu, *Science* **292**, 90 (2001).
13. J. E. Walsh, W. L. Chapman, T. L. Shy, *J. Clim.* **9**, 480 (1996).
14. D. W. J. Thompson, J. M. Wallace, G. Hegerl, *J. Clim.* **13**, 1018 (2000).
15. S. B. Feldstein, *J. Clim.* **15**, 88 (2002).
16. I. G. Rigor, R. L. Colony, S. Martin, *J. Clim.* **13**, 896 (2000).
17. R. Kwok, D. A. Rothrock, *J. Geophys. Res.* **104**, 5177 (1999).
18. R. Kwok, *Geophys. Res. Lett.* **27**, 775 (2000).
19. I. G. Rigor, J. M. Wallace, R. L. Colony, *J. Clim.* **15**, 2648 (2002).
20. J. Zhang, D. Rothrock, M. Steele, *J. Clim.* **13**, 3099 (2000).
21. M. Hilmer, T. Jung, *Geophys. Res. Lett.* **27**, 989 (2000).
22. C. L. Parkinson *et al.*, *J. Geophys. Res.* **104**, 20837 (1999).
23. R. R. Dickson, *Nature* **397**, 389 (1999).
24. C. Deser, *Geophys. Res. Lett. 27*, 779 (2000).
25. M. H. P. Ambaum, B. J. Hoskins, D. B. Stephenson, *J. Clim.* **14**, 3495 (2001).
26. J. M. Wallace, D. W. J. Thompson, *Phys. Today* **55** (no. 2), 28 (February 2002).
27. D. W. Thompson, S. Lee, M. P. Baldwin, *Monograph on the North Atlantic Oscillation* (American Geophysical Union, Washington, DC, in press).
28. D. W. J. Thompson, J. M. Wallace, *J. Clim.* **13**, 1000 (2000).
29. S. Manabe, R. J. Stouffer, *J. Geophys. Res.* **85**, 5529 (1980).
30. _____, M. J. Spellman, K. Bryan, *J. Clim.* **4**, 785 (1991).
31. S. J. Manabe, R. J. Stouffer, *J. Clim.* **9**, 376 (1996).
32. I. V. Polyakov *et al.*, *Geophys. Res. Lett.*, in press.
33. T. L. Delworth, T. R. Knutson, *Science* **287**, 2246 (2000).
34. J. Overpeck *et al.*, *Science* **278**, 1251 (1997).
35. P. A. Mayewski *et al.*, *Science* **232**, 975 (1986).
36. W. L. Chapman, J. E. Walsh, *Bull. Am. Meteorol. Soc.* **74**, 33 (1993).
37. J. M. Wallace, Y. Zhang, L. Bajuk, *J. Clim.* **9**, 249 (1996).
38. T. Delworth, S. Manabe, R. J. Stouffer, *J. Clim.* **6**, 1993 (1993).
39. C. Mauritzen, S. Hakkinen, *Geophys. Res. Lett.* **24**, 3257 (1997).
40. M. M. Holland, C. Bitz, M. Eby, A. Weaver, *J. Clim.* **14**, 656 (2001).
41. Intergovernmental Panel on Climate Change, *IPCC Third Assessment Report. Climate Change 2001: The Scientific Basis* (Cambridge Univ. Press, Cambridge, 2001).
42. J. K. Kahl, D. J. Charlevoix, N. A. Zaitseva, R. C. Schnell, M. C. Serreze, *Nature* **361**, 335 (1993).
43. J. Haywood, R. Stouffer, R. Wetherald, S. Manabe, V. Ramaswamy, *Geophys. Res. Lett.* **24**, 1335 (1997).
44. S. F. B. Tett, P. Stott, M. Allen, W. Ingram, J. Mitchell, *Nature* **399**, 569 (1999).
45. J. Weatherly, C. Bitz, *12th Symp. Global Change and Clim. Variations*, American Meteorological Society, 15 to 18 January 2001, Albuquerque, NM (American Meteorological Society, Boston, 2001).
46. C. M. Bitz, G. Roe, in preparation.
47. M. Baldwin, T. Dunkerton, *J. Geophys. Res.* **104**, 30937 (1999).
48. I. M. Held, in *Large-Scale Dynamical Processes in the Atmosphere*, B. Hoskins, R. Pearce, Eds. (Academic Press, London, 1983), chap. 6, pp. 127–168.
49. J. Perlwitz, H. Graf, *J. Clim.* **8**, 2281 (1995).
50. D. G. Andrews, J. R. Holton, C. B. Leovy, *Middle Atmosphere Dynamics* (Academic Press, New York, 1987).
51. E. DeWeaver, S. Nigam, *J. Clim.* **13**, 2160 (2000).
52. V. Limpasuvan, D. Hartmann, *Geophys. Res. Lett.* **26**, 3133 (1999).
53. P. Chen, W. Robinson, *J. Atmos. Sci.* **49**, 2533 (1992).
54. J. G. Charney, P. G. Drazin, *J. Geophys. Res.* **66**, 83 (1961).
55. R. X. Black, *J. Clim.* **15**, 268 (2002).
56. H. Graf, J. Perlwitz, I. Kirchner, I. Schult, *Contrib. Phys. Atmos.* **68**, 233 (1995).
57. N. P. Gillett *et al.*, *J. Geophys. Res.* **107**, 1 (2002).
58. N. P. Gillett, M. R. Allen, K. D. Williams, *Geophys. Res. Lett.* **29**, 14444 (2002).

59. E. Maloney, D. Hartmann, *J. Clim.* **14**, 2015 (2001).
60. M. E. Mann, R. S. Bradley, M. K. Hughes, *Nature* **392**, 779 (1998).
61. _____, *Geophys. Res. Lett.* **26**, 759 (1999).
62. J. Esper, E. R. Cook, F. H. Schweingruber, *Science* **295**, 2250 (2002).
63. D. W. J. Thompson, S. Solomon, *Science* **296**, 895 (2002).
64. D. P. Schneider, E. J. Steig. *Geophys. Res. Lett.*, in press.
65. C. Appenzeller, T. F. Stocker, M. Anklin, *Science* **282**, 446 (1998).
66. J. Luterbacher *et al.*, *Geophys. Res. Lett.* **26**, 2745 (1999).
67. E. R. Cook, R. D'Arrigo, K. Briffa, *Holocene* **8**, 9 (1998).
68. L. Tremblay, L. A. Mysak, A. S. Dyke, *Geophys. Res. Lett.* **24**, 2027 (1997).
69. C. Schmutz *et al.*, *Geophys. Res. Lett.* **27**, 1135 (2000).
70. G. Bond *et al.*, *Science* **294**, 2130 (2001).
71. S. R. O'Brien *et al.*, *Science* **270**, 1962 (1995).
72. T. J. Crowley, *Quat. Res.* **21**, 105 (1984).
73. D. T. Shindell *et al.*, *Science* **294**, 2149 (2001).
74. P. M. Grootes *et al.*, *Nature* **366**, 552 (1993).
75. J. P. Sachs, S. J. Lehman, *Science* **286**, 756 (1999).
76. L. Stott, C. Poulsen, S. Lund, R. Thunell, *Science* **297**, 222 (2002).
77. A. Koutavas, J. Lynch-Stieglitz, T. M. Marchitto Jr., J. P. Sachs, *Science* **297**, 226 (2002).
78. W. S. Broecker, *Science* **278**, 1582 (1997).
79. C. D. Charles, R. G. Fairbanks, *Nature* **355**, 416 (1992).
80. J. F. Adkins *et al.*, *Science* **280**, 725 (1998).
81. L. D. Keigwin, E. A. Boyle, *Proc. Natl. Acad. Sci. U.S.A.* **97**, 1343 (2000).
82. G. A. Meehl, J. M. Arblaster, W. G. Strand Jr., *Clim. Dyn.* **16**, 257 (2000).
83. D. Rind, R. Healy, C. Parkinson, D. Martinson, *J. Clim.* **8**, 449 (1995).
84. _____, *Geophys. Res. Lett.* **24**, 1491 (1997).
85. M. M. Holland, C. M. Bitz, in preparation.
86. P. D. Jones, *J. Clim.* **7**, 1794 (1994).
87. E. Kalnay *et al.*, *Bull. Am. Meteorol. Soc.* **77**, 437 (1996).
88. G. A. Meehl, G. J. Boer, C. Covey, M. Latif, R. J. Stouffer, *Bull. Am. Meteorol. Soc.* **81**, 313 (2000).
89. We thank J. Walsh, D. Hartmann, G. Roe, J. Morison, and one anonymous reviewer for helpful comments. This research was supported by the NSF through grant OPP0084287.

REVIEW

Mass Balance of Polar Ice Sheets

Eric Rignot[1] and Robert H. Thomas[2]

Recent advances in the determination of the mass balance of polar ice sheets show that the Greenland Ice Sheet is losing mass by near-coastal thinning, and that the West Antarctic Ice Sheet, with thickening in the west and thinning in the north, is probably thinning overall. The mass imbalance of the East Antarctic Ice Sheet is likely to be small, but even its sign cannot yet be determined. Large sectors of ice in southeast Greenland, the Amundsen Sea Embayment of West Antarctica, and the Antarctic Peninsula are changing quite rapidly as a result of processes not yet understood.

The Antarctic and Greenland ice sheets together hold 33 million cubic km of ice, representing enough water to raise global sea level by 70 m. Annual snowfall on the ice sheets is equivalent to 6.5 mm of sea level, so that only a small imbalance between snowfall and discharge of ice and meltwater into the ocean could be a major contributor to present-day sea-level rise [~1.8 mm/year (*1*)]. Large variations in sea level over the past million years have in fact been controlled by ice, with rates of sea-level rise at least one order of magnitude larger than at present during times of rapid deglaciation. Consequently, a detailed knowledge and understanding of the evolution of polar ice sheets is of considerable societal importance, and here we review current progress based on observations made during the last decade.

The balance between net accumulation and attrition of ice is not the same for the two ice sheets, owing to differences in climatic regime. Antarctica has a dominant influence on its own climate and on the surrounding ocean, with cold conditions even during the summer and around its northern margins, so there is little surface melting, even near the coast. Vast floating ice shelves exist around much of the periphery of the continent, fed in part by ice discharged from the ice sheet by outlet glaciers and ice streams, some penetrating deep into the heart of Antarctica. Ice is lost primarily by basal melting and iceberg calving from these ice shelves.

By contrast, Greenland's climate is strongly affected by nearby land masses and the North Atlantic, with the Gulf Stream to the south. The average accumulation rate (~30 cm/year) is twice that for Antarctica. Summer melting occurs over half of the ice-sheet surface, with much of the water flowing to the sea. The ice sheet is fringed almost completely by coastal mountains through which it is drained by many glaciers. Ice is lost primarily by surface runoff and iceberg calving, except in the north where basal melting from small ice shelves is substantial.

These ice sheets were much larger at the last glacial maximum, some 21,000 years ago, retreating to their present condition in the last few thousand years. Their present mass balance depends on this long-term trend, determined by past climate and dynamic history, and on more recent changes in climate and ice-sheet dynamics. A major challenge of modern glaciology is to separate the long-term background signal from more recent changes.

Ice-Sheet Mass Balance

There are three ways to measure the mass balance of an ice sheet:

(i) The mass budget method, which compares losses by melting and ice discharge with total net input from snow accumulation. Net accumulation is inferred primarily from ice-core measurements, with 5% errors for large-area averages (*2*–*4*). Loss by melting is more complex because of meltwater refreezing after draining into near-surface snow (*5*). Melt rates are commonly estimated from positive degree-day models (*6*). Although large uncertainties suggest that accurate mass-balance determination for an entire ice sheet is difficult by the mass budget method, it can be achieved for smaller regions by measuring ice discharge inland of the grounding line, an approach made possible by new techniques for measuring ice velocities over large areas from Global Positioning System (GPS) and interferometric synthetic-aperture radar (InSAR) data, provided that ice thickness is known.

(ii) Measurements of elevation change over time, which are translated into measurements of volume change by including estimates of the vertical motion of underlying ground associated with isostatic rebound or tectonics. Satellite radar altimeters (Seasat, Geosat, and European Remote Sensing Satellites ERS-1 and -2) have been used to infer elevation change rates over Greenland and Antarctica since 1978 (*7, 8*). Coverage is limited to the interior regions of the ice sheets, where surface slopes are low. Aircraft altimeters were used extensively over Greenland in the 1990s (*9*). Launch of NASA's Ice, Cloud, and Land Elevation Satellite (ICESat), with a laser altimeter and orbit coverage to 86°S, and the European Cryosat, with a small-footprint radar altimeter extending to 88°S, will increase measurement accuracy and extend surveys to the interior regions and to the ice-sheet margins, where remote sensing measurements are most challenging and thickness changes are most pronounced.

(iii) Weighing of the ice sheets. NASA's

[1]Jet Propulsion Laboratory, California Institute of Technology, Mail Stop 300-235, Pasadena, CA 91109, USA. [2]EG&G Services, Wallops Flight Facility, Building N-159, Wallops Island, VA 23337, USA. E-mail: eric@adelie.jpl.nasa.gov, robert_thomas@hotmail.com